analytical chemistry

Article

pubs.acs.org/ac

Rapid Slow Off-Rate Modified Aptamer (SOMAmer)-Based Detection of C-Reactive Protein Using Isotachophoresis and an Ionic Spacer

Charbel Eid,[†] James W. Palko,[†] Evaldas Katilius,[§] and Juan G. Santiago*[,†]

[†]Department of Mechanical Engineering, Stanford University, Stanford, California 94305, United States

[§]SomaLogic, Inc., Boulder, Colorado 80301, United States

Supporting Information

ABSTRACT: We present an on-chip electrophoretic assay for rapid protein detection with a SOMAmer (Slow Off-Rate Modified Aptamer) reagent. We used isotachophoresis (ITP) coupled with an ionic spacer to both react and separate SOMAmer–protein complex from free SOMAmer reagent. ITP accelerates the reaction kinetics as the ionic spacer concurrently separates the reaction products. We developed a numerical and analytical model to describe ITP spacer assays, which involve low-mobility, nonfocusing targets that are recruited into the ITP zone by higher-mobility, ITP-focused probes. We demonstrated a proof-of-concept of this assay using C-reactive protein (CRP) in buffer, and achieved a 2 nM limit of detection (LOD) with a combined 20 min assay time (10 min off-chip preparation of reagents and 10 min on-chip run). Our findings suggest that this approach has potential as a simple and rapid alternative to other homogeneous immunoassays. We also explore the extension of this assay to a diluted serum sample spiked with CRP, where we observe decreased sensitivity (an LOD of 25 nM in 20-fold diluted serum). We describe the challenges in extending this assay to complex samples and achieving higher sensitivity and specificity for clinical applications.

Protein diagnostic assays are increasingly popular in molecular diagnostics.[1−3] Because of their diverse roles in the majority of the body's mechanisms, protein biomarkers hold revealing information about many bodily processes and pathologies.[4] The plasma proteome is particularly vast, containing plasma proteins as well as tissue proteins and a variety of immunoglobulins. For example, because they transmit immediate information about phenotype, plasma proteins are especially attractive in medical diagnostics.[5,6]

Currently, the two leading techniques for protein quantification are mass spectrometry and antibody assays. Mass spectrometry is able to resolve complex samples with high fidelity. However, it is a time-consuming and laborious approach that involves several manual steps. Mass spectrometry is also highly sensitive to a large number of detergents and polymers commonly used in sample preparation.[7] Antibody-based assays, on the other hand, offer high sensitivity and specificity, and have been accepted as a "gold standard" in protein biomarker detection and quantification. However, immunoassays are limited by the availability and quality (e.g., affinity) of available antibodies targeting specific proteins. Furthermore, antibodies are very sensitive to factors such as temperature and pH, and can undergo irreversible denaturation.[8]

Aptamers are synthetic nucleic acid (NA) ligands and a promising alternative to antibodies for protein detection.[9] Developed through several rounds of a process known as SELEX,[10] aptamers are synthesized using solid-state DNA synthesis methods allowing for reproducible replenishment of reagents, typically a problem with antibodies. DNA-based aptamers also tend to be more stable and can be reversibly denatured by heat. However, performance of traditional aptamers has been hamstrung by several issues, including relatively low affinity and high dissociation rates (k_{off}). In an effort to address these deficiencies of aptamers, SomaLogic, Inc. has developed SOMAmers (Slow Off-Rate Modified Aptamers),[11,12] which use modified nucleotide bases which offer expanded chemical diversity for interactions, in particular hydrophobic groups similar to amino acid residues. Modifications on nucleotides also dramatically improve ability to select SOMAmers for various protein targets with excellent (sub-nM) affinity. Standard on-chip capillary electrophoresis (CE)[13,14] and chromatography techniques[15,16] for aptamer-type detection have been used with some success, but are often impractical because they do not allow sample recovery and can require long separation times.

Recent work has been aimed at electrokinetic aptamer-based detection of proteins on microfluidic chips. Wang et al.[17] used transient isotachophoresis (t-ITP) with a modified TE to detect thrombin–aptamer complexes at an intersection. Their assay had a 1 nM LOD. However, t-ITP is subject to significant dispersion effects, reducing the signal-to-noise ratio. Cheow et al.[18] designed a chip in which conductivity gradients were created on the boundaries of ion depletion zones. Aptamer and protein targets were reacted off-chip, then continuously injected into the channel. Free aptamer and aptamer–protein complexes were focused at different locations of the conductivity gradient, allowing the detection and quantification

Received: March 5, 2015
Accepted: May 29, 2015

DOI: 10.1021/acs.analchem.5b00886
Anal. Chem. XXXX, XXX, XXX−XXX

of complexes. Although this approach achieved high sensitivity, the assay required separate off-chip incubation, followed by on-chip signal enhancement and a total assay time of 60 min. The authors found the separation resolution to vary based on assay conditions. They suggested the addition of a spacer may better control the separation resolution between the two peaks.

In this work, we present a novel assay for ITP-based detection of a protein target with a SOMAmer probe. ITP is an electrophoretic technique that can selectively purify and preconcentrate reactants at a sharp interface, allowing isolation and concentration of low abundance probe-target complexes and increasing complex forming reaction kinetics.[19] ITP uses a discontinuous buffer consisting of a high-mobility leading electrolyte (LE) and a low-mobility trailing electrolyte (TE).While migrating in an electric field, analytes with mobilities intermediate to those of the LE and TE focus at the TE/LE interface. Recently, ITP has been used in conjunction with a separation modality to react and subsequently separate reaction products. Garcia-Schwarz and Santiago[20,21] combined ITP with gel-immobilized NA capture probes to purify and detect miRNA with high sensitivity and specificity. Bahga et al.[22] used bidirectional ITP and CE to react and separate DNA reaction products. Han et al.[23] extended ITP-aided hybridization to microarrays, achieving almost an 8-fold increase in signal in their 30 min assay (as compared with overnight incubation assays).

ITP has been leveraged in the acceleration of reactions with protein targets. Khnouf et al.[24] used ITP to accelerate heterogeneous immunoassays in which antibodies were bound to magnetic beads or to the channel wall. Kawabata et al.[25] leveraged ITP for accelerated reaction and separation in an α-fetoprotein immunoassay. This assay was later developed into a commercial product by Wako Pure Chemical Industries and validated in clinical samples.[26] We note that, with the exception of the α-fetoprotein immunoassay, the use of ITP to accelerate reactions in complex samples has largely been limited to NAs rather than protein assays.[21,27] High protein content in samples such as serum (60−80 g/L) can result in protein precipitation, nonspecific interactions, and other deleterious effects. In this study, we briefly explore challenges of extending ITP to protein assays in complex samples.

In the assay reported here, we leverage the two standard modes of ITP: peak mode and plateau mode. Peak mode usually occurs when analyte concentrations are several orders of magnitude smaller than those of the LE and TE buffers. In peak mode, analytes focus at a sharp interface between the LE and TE, and have a negligible effect on the local ionic conductivity in the channel.[28] Above a certain threshold concentration, the analyte eventually segregates into a plateau-like zone of constant concentration and increasing length.[29] Plateau-mode ITP has been leveraged to separate and indirectly detect nonfluorescent species.[30,31] We recently demonstrated an assay in which we integrated peak and plateau-mode ITP.[32] In the first stage, we used peak-mode ITP to preconcentrate and mix DNA probe and target molecules at a sharp interface. In the second stage, using a region with sieving matrix and an ionic spacer with mobility between that of the probe and target, we triggered plateau-mode ITP and separated the excess probe from the probe−target complex. We achieved a limit of detection of 220 fM, the highest reported sensitivity for free solution NA-based ITP assays.

We present an integrated assay to detect a low-mobility protein target using ITP and an ionic spacer. We know of no other work that has extended ITP-based reaction assays to nonfocusing, low-mobility targets, in which higher-mobility probe molecules recruit target molecules into the ITP zone. Our assay is carried out in a microfluidic channel, allowing reaction of protein and SOMAmer and detection of the protein−SOMAmer complex on the same chip. We demonstrate the applicability of ITP-spacer assays to generally nonfocusing targets. In addition, we present a simple analytical model describing the reaction, as well as design considerations broadly applicable to ITP-spacer assays with low-mobility, nonfocusing targets. We demonstrate a proof-of-concept assay with C-reactive protein (CRP) as a clinically relevant protein target. Lastly, we perform preliminary experiments to explore the extension our assay to detect CRP in a serum sample. We discuss challenges and recommendations for enhancing the performance of this assay in complex samples.

PRINCIPLE OF THE ASSAY

Figure 1 presents an overview of this assay. We inject the fluorescently labeled SOMAmer and protein molecules in the channel, within the LE buffer. We then load the TE and spacer into the TE reservoir. Upon applying current, the LE, TE, spacer, SOMAmer reagent, and CRP target all begin to migrate toward the cathode (LE reservoir). An ITP peak consisting of SOMAmer forms immediately outside the TE reservoir. The high concentration of SOMAmer focused by ITP at the LE/

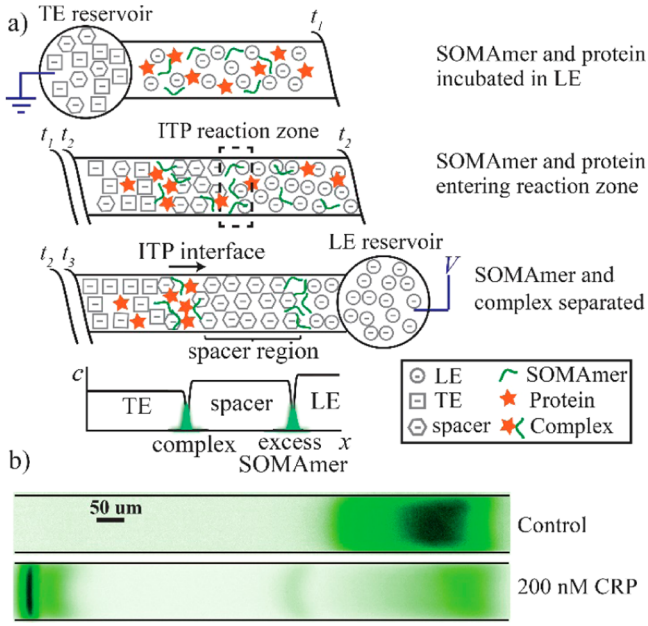

Figure 1. (a) Schematic representation of the ITP−spacer assay. At t_1, the AlexaFluor 488-labeled SOMAmer reagent and the protein target are loaded in the LE buffer, while the TE and spacer ions are loaded into the TE reservoir. At t_2, ITP is initiated. Low-mobility complexes are formed by binding of SOMAmers and targets and then oversped by spacer molecules. At t_3, unreacted SOMAmer molecules are focused between the LE and spacer, whereas SOMAmer−target complexes are focused at the interface between the spacer and TE. (b) Experimental visualization of the ITP-spacer assay in the detection region. In the negative control case, where only SOMAmer reagent is included, we observe only one ITP peak for free SOMAmer reagent. When 200 nM of CRP is included in the mixture, a second ITP peak forms at the trailing spacer/TE interface. This trailing peak represents the focused SOMAmer−target complex.

DOI: 10.1021/acs.analchem.5b00886
Anal. Chem. XXXX, XXX, XXX−XXX

spacer interface accelerates the second-order reaction kinetics between the SOMAmer and CRP in this region. Concurrently, SOMAmer and CRP molecules bind in the LE zone. As SOMAmer−CRP complexes form, they are overtaken by spacer molecules, which have higher mobility than that of the SOMAmer−CRP complex but lower than that of free SOMAmer. The complex refocuses at the spacer-TE interface, separating from the free SOMAmer and forming a trailing second peak, allowing detection of CRP in the labeled complex. Because of the large difference in mobility between the free SOMAmer and SOMAmer/CRP complex, no sieving matrix is needed in this assay. The simultaneous reaction and separation processes continue as the species migrate along the channel and reach the detection point where the SOMAmer/CRP complex concentration is measured.

THEORY

We present an analysis of the reaction and separation processes which occur in an ITP−spacer assay with a nonfocusing target, as well as recommendations on assay design. We begin with a simplified model of the probe-target reaction similar to the analysis of Bercovici and Han.[33] In this model, we assume that the dissociation constant $K_d \ll 1\ \mu$M, such that dissociation rate k_{off} is much smaller than the characteristic association rate $k_{on}c_{P,0}$ where k_{on} is the association rate constant and $c_{P,0}$ is the initial probe concentration. We load both the probe (SOMAmer) and target (CRP) in the LE zone (Figure 1a). There are thus two regions where the probe−target reactions occur: in the LE zone (containing unfocused reactants) and in the ITP zone. The LE zone reactions are given by

$$\begin{cases} \dfrac{dc_P^{LE}}{dt} = -k_{on}c_P^{LE}c_T^{LE} \\ \dfrac{dc_T^{LE}}{dt} = -k_{on}c_P^{LE}c_T^{LE} \\ \dfrac{dN_{PT}^{LE}}{dt} = k_{on}c_P^{LE}c_T^{LE}V(t) \end{cases} \quad (1)$$

where $V(t) = A(L_0 - U_{ITP}t)$ is the time-dependent volume of the LE zone. U_{ITP} is the velocity of the ITP front, A is the channel's cross-sectional area, and L_0 is the length of the channel. As the ITP zone migrates through the channel, the volume of the LE zone continuously decreases. Reactions in the ITP zone are given by

$$\begin{cases} \dfrac{dc_P^{ITP}}{dt} = -k_{on}c_P^{ITP}c_T^{ITP} + \dfrac{U_{ITP}}{\delta}\eta_{P,LE}c_P^{LE} \\ \dfrac{dc_T^{ITP}}{dt} = -k_{on}c_P^{ITP}c_T^{ITP} + \dfrac{U_{ITP}}{\delta}\eta_{T,LE}(c_T^{LE} - c_T^{ITP}) \\ \dfrac{dN_{PT}^{ITP}}{dt} = k_{on}c_P^{ITP}c_T^{ITP}(\delta A) \end{cases} \quad (2)$$

where $\eta_{P,LE} = 1 - \mu_P/\mu_{LE}$ and $\eta_{T,LE} = 1 - \mu_T/\mu_{LE}$. Parameters c_P and c_T represent the concentrations of probe and target, respectively. N_{PT} is the number of probe target complexes present. Superscripts "LE" and "ITP" designate the LE and ITP zones, respectively. δ represents the characteristic axial width of the ITP peak, and μ represents electrophoretic mobility. $\eta_{P,LE}$ and $\eta_{T,LE}$ represent the normalized difference in mobility between the LE and the probe and target, respectively. Here, the subscripts "P", "T", "PT", "LE", "TE", "spacer", and "CI" denote properties related to the probe, target, probe-target complex, LE, TE, spacer, and counterion, respectively. We note that all species mobilities refer to the mobility of that species in the buffer in which it is migrating (e.g., μ_T refers to the mobility of the target in the LE buffer).

Probe molecules continuously accumulate in the ITP zone at a rate proportional to the relative difference in mobility between the LE and the probe, $\eta_{P,LE}$. Target molecules do not focus in ITP, but instead enter the ITP zone from the LE and exit to the spacer and TE zones. In addition to the fundamental requirements necessary for all ITP assays ($\mu_{LE} > \mu_{TE}$ in their respective zones), an ITP−spacer reaction−separation assay requires that $\mu_P > \mu_{spacer} > \mu_{PT} > \mu_{TE}$. In this analysis, we assume that $\mu_{TE} > \mu_T$, since the target does not focus in ITP.

Production of the Probe−Target Complex in the Channel. In this section, we focus on the case where the probe is abundant, with respect to the target, because this is often the most interesting regime for biomolecule detection assays. Therefore, we assume that $c_{P,0} \gg c_{T,0}$, which simplifies the model presented above. We present the simplified model in the Supporting Information. During the assay, probe−target complexes form in the ITP and LE zones. As the ITP zones sweep through the channel, the formed probe−target complexes accumulate at the spacer/TE interface. The rate of product formation per unit volume is significantly higher in the ITP zone at the interface between the LE and spacer. However, the LE zone occupies a much larger volume than the ITP zone, and so its production of product cannot be neglected. We find that, for the current assay design and a wide range of assay parameters, the rates of complex formation in the LE and ITP zones are on the same order of magnitude and both should be considered. There exists an interesting tradeoff between reducing assay time and producing a large number of probe−target complexes. We introduce the nondimensional parameter λ to quantify this tradeoff. λ relates the assay velocity, channel length, association on-rate, and initial probe concentration:

$$\lambda = \frac{L_0 k_{on} c_{P,0}}{U_{ITP}} \quad (3)$$

λ can be interpreted as a modified Damköhler number, relating the advection and the reaction rates. Under the simplifying assumptions listed above, λ incorporates several of the key variables influencing complex formation and determines the fraction of target molecules which are bound and can be detected at the end of the assay. In Figure 2, we visualize the relationship between complex formation and λ, which shows sigmoidal character. At low λ values, the free probes are swept away by the ITP zone before they have a chance to bind with target. Conversely, at high λ values, the reaction between probe and target molecules approaches equilibrium in the LE, minimizing the effect of ITP on reaction kinetics. The optimal region of operation is at the very beginning of the plateau at higher λ, which maximizes product formation while minimizing assay time.

Spacer Zone Length and Complex Accumulation. In order to be detected, probe−target complexes must be separated from excess probes and focused at a separate ITP interface. The probe−target complex forms in the LE and ITP reaction zones, is oversped by the LE and spacer molecules, and refocuses at the trailing spacer/TE interface. In this section, we present an analysis of the competing phenomena of spacer zone growth and complexes falling behind the spacer molecules and

DOI: 10.1021/acs.analchem.5b00886
Anal. Chem. XXXX, XXX, XXX−XXX

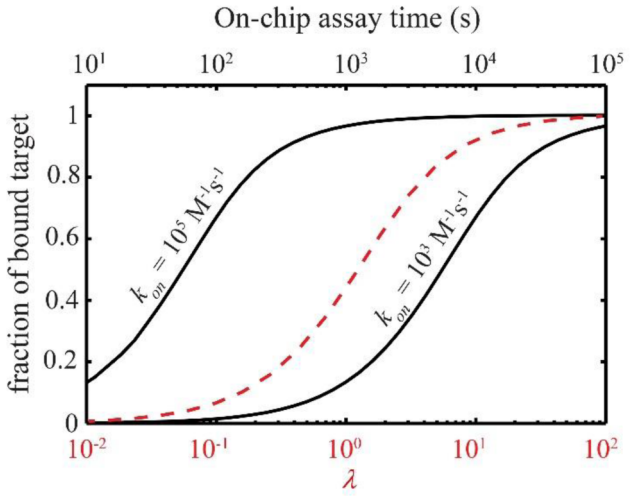

Figure 2. Results of analytical modeling determining the fraction of bound, detectable target at the end of the assay for the case with abundant probe. We show the ratio of target molecules which have formed a complex as a function of λ, ITP assay times, and k_{on} values. The dashed curve represents the bound target as a function of parameter λ (see eq 3). We find a sigmoidal shape and a region of assay times that maximizes complex formation while minimizing assay time. The assay temporal response curves over different values of k_{on} collapse into a single λ curve. We experimentally measure the assay time to be ~600 s in a 45-mm-long channel. We use an initial SOMAmer concentration of 180 nM. We assume $\mu_{LE} = -79 \times 10^{-9}$ m^2 V^{-1} s^{-1} (that of the commonly used Cl^-), $\mu_P = -30 \times 10^{-9}$ m^2 V^{-1} s^{-1}, and $\mu_T = -2 \times 10^{-9}$ m^2 V^{-1} s^{-1}, and an ITP zone width of 100 μm.

accumulating at the trailing interface. As discussed earlier, plateau ITP is triggered when the spacer reaches a threshold concentration, above which the spacer molecules cease to accumulate in a high-concentration peak and instead form a growing zone. This plateau concentration is given by Martin and Everaerts:[34]

$$c_{spacer}^{threshold} = c_{LE}\frac{\mu_{spacer}(\mu_{LE} - \mu_{CI})}{\mu_{LE}(\mu_{spacer} - \mu_{CI})}\left(\frac{z_{LE}}{z_{spacer}}\right) \quad (4)$$

where z indicates the molecule's ionic charge. We can decrease the time needed to induce plateau mode by loading a larger concentration of spacer into the TE reservoir and/or including a lower concentration of LE in the channel. Above the threshold concentration, the newly formed spacer plateau zone grows proportionally to the influx of spacer molecules at the ITP interface. This rate is given by Martin and Everaerts:[34,35]

$$\frac{dL_{spacer}}{dt} = \frac{\mu_{LE}}{\mu_{TE}}\left[\frac{(\mu_{spacer} - \mu_{TE})(\mu_{spacer} - \mu_{CI})}{\mu_{spacer}(\mu_{LE} - \mu_{CI})}\right]\left(\frac{c_{spacer}^{well}}{c_{LE}}\right)V_{ITP} \quad (5)$$

L_{spacer} represents the length of the growing spacer zone and c_{spacer}^{well} denotes the concentration of the spacer species in the TE reservoir. The length of the LE-filled channel gives the upper bound for L_{spacer}, while its lower limit is dependent on the ability of the detector to distinguish between the LE/spacer and spacer/TE interfaces, where the unbound and bound probes are focused, respectively.

While the spacer zone grows in length as described above, the probe−target complex traverses the spacer zone and accumulates at the spacer/TE interface. The rate at which the probe−target complex migrates backward (in the ITP frame of reference) toward the trailing ITP zone is given by

$$V_{spacer} - V_{PT} = V_{ITP}\left(1 - \frac{\mu_{PT}}{\mu_{spacer}}\right) \quad (6)$$

where V_{PT} and V_{spacer} are the velocities of the probe−target complex and spacer in the spacer zone. Therefore, in order to ensure that the probe−target complex is approaching the spacer/TE interface (eq 6) faster than the spacer zone is growing (eq 5), we consider the ratio of eqs 5 and 6. We define this ratio as

$$\alpha = \frac{\mu_{TE}}{\mu_{LE}}\left(\frac{\mu_{spacer} - \mu_{PT}}{\mu_{spacer} - \mu_{TE}}\right)\left(\frac{\mu_{LE} - \mu_{CI}}{\mu_{spacer} - \mu_{CI}}\right)\frac{c_{LE}}{c_{spacer}^{well}} \quad (7)$$

For large values of α ($\alpha \gg 1$), the rate of probe−target complex accumulation is significantly greater than the rate of growth of the spacer zone, and the large majority of complexes are focused at the spacer/TE interface for detection with relatively few left in the spacer zone. In practice, probe−target complex mobility may be difficult to determine for this calculation. However, NA−protein complexes generally migrate at a lower mobility than the free NAs.[36,37] If the probe−target complex mobility is unknown, we recommend using a high-mobility spacer, increasing LE concentration, or reducing the spacer reservoir concentration to increase the fraction of formed probe−target complexes that are focused at the trailing interface. Generally, a slower probe−target complex results in faster accumulation (larger α values). In Table 1, we summarize the influence of several important parameters on the design of a high-performance ITP−spacer reaction−separation assay.

MATERIALS AND METHODS

Chip and Reagents. All experiments were performed on a 20-μm-deep Crown glass NS-12A chip (Figure 3) from Caliper Life Sciences (Mountain View, CA). The channels are 90 μm

Table 1. Important Parameters in ITP−Spacer Assay Design

parameter	interpretation	notes
μ_{LE}	mobility of the LE ion	choosing $\mu_{LE} \gg \mu_T$ and $\mu_{LE} \gg \mu_P$ maximizes flux of probe and target molecules into the ITP reaction zone
μ_{spacer}, c_{spacer}^{well}	mobility of spacer ion and reservoir spacer concentration	maximizing $\mu_{spacer} - \mu_{TE}$ and c_{spacer}^{well} minimizes the flux of probe−target complex molecules out of the ITP reaction zone
λ	ratio of convective to reactive time scales	when probe is abundant and $k_{off} \ll k_{on}$, λ collapses the effect of several assay parameters on complex production
α	ratio of complex accumulation rate to spacer zone growth rate	if $\alpha \gg 1$, probe−target complexes reach the spacer/TE interface at a higher rate than the spacer molecules

DOI: 10.1021/acs.analchem.5b00886
Anal. Chem. XXXX, XXX, XXX−XXX

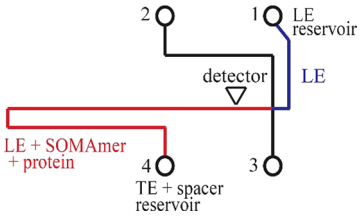

Figure 3. Design of the Caliper NS12 deep Crown glass chip. Prior to each run, a section of the channel is filled with pure LE buffer (blue) and another section is filled with LE buffer mixed with SOMAmer and protein (red). The detection point is placed ~5 mm away from the cross junction (as shown). ITP proceeds from reservoir 4 to reservoir 1.

wide and 20 μm deep. The SOMAmer/protein injection region between reservoir 4 and the cross junction is 45 mm in length. The detection point was located ~5 mm away from the cross-junction.

For ITP hybridization, we prepared an LE buffer consisting of 100 mM HCl, 200 mM imidazole (pK_a = 7.15), 1% (w/v) PVP, 0.02% (v/v) Tween-20, 6 mM $MgCl_2$, and 10 μM of the nonspecific blocker, Z-block. PVP was used to suppress electro-osmotic flow. Tween-20 was included to increase protein solubility and minimize nonspecific adsorption of the protein target to the walls of the microfluidic channel. Mg^{2+} was used to ensure appropriate binding between the SOMAmer and the target protein. We use imidazole as the counterion, because of its pK_a value, which is close to the physiological pH (~7.4), which is optimal for SOMAmer binding. Z-block is a synthetic oligodeoxynucleotide containing Benzyl-dU modified bases, synthesized at SomaLogic.[38] We include it in high concentrations to act as a competitive inhibitor of nonspecific interactions. We mixed both the SOMAmer and CRP with the LE buffer. The TE consisted of 100 mM tricine, 200 mM imidazole, 0.5 mM HEPES, and 1% PVP. HEPES acted as a spacer in these experiments. We determined the appropriate spacer through an iterative process.

We prepared serum samples from whole blood samples in nonanticoagulated tubes donated by healthy donors to the Stanford Blood Center (Palo Alto, CA). The fresh human blood samples clotted for approximately an hour at room temperature. We then removed the clot by centrifuging at 1500*g* for 15 min. We collected and made aliquots of the resultant supernatant serum. Serum samples were then stored at −80 °C. We note that, for experiments with the serum sample, we used 0.2% (v/v) Triton X-100 as a surfactant instead of Tween-20, because of decreased aggregate formation with Triton X-100.

We purchased HEPES, Tris, imidazole, PBS, tricine, glycerol, Tween-20, and Triton X-100 from Sigma−Aldrich (St. Louis, MO). Magnesium chloride was obtained from EMD Millipore (Gibbstown, NJ). Polyvinylpyrrolidone (PVP, MW = 1 000 000) was purchased from Polysciences, Inc. (Warrington, PA). Hydrochloric acid was procured from J.T. Baker (Avantor Performance Materials, Center Valley, PA). AlexaFluor 488-labeled SOMAmer (AF488-SOMAmer) and Z-block were provided by SomaLogic, Inc. (Boulder, CO). C-reactive protein was obtained from US Biological (Salem, MA). SOMAmers were stored in a buffer consisting of 10 mM HCl and 20 mM Tris. The stock solutions were stored at −20 °C, but a working stock was stored at 4 °C and replaced every 2 days. CRP was stored in a solution consisting of 0.8x PBS (phosphate buffered saline) and 50% (v/v) glycerol. Glycerol was used in order to prevent the protein from freezing while being stored at −20 °C, and its subsequent denaturation. Other solutions were stored at room temperature. All solutions were prepared in DNase/RNase-free distilled water (GIBCO Invitrogen, Carlsbad, CA).

Protocol and Chip Operation. Prior to and between each experiment, we prepared the channel with the following wash protocol: deionized water (DI) for 1 min, 1 M NaOH for 1 min, DI for 1 min, 1 M HCl for 1 min, and finally DI for 1 min. We used this protocol to remove adsorbed proteins and impurities from the channel. We then filled all reservoirs with LE buffer and applied a vacuum at reservoir 2 (Figure 3) to fill the entire channel with LE. Prior to each run, we mixed the SOMAmer in the LE buffer (and serum when working with the serum sample), heated the solution at 95 °C for 10 min, and then allowed to cool to room temperature, as recommended by SomaLogic. This was done to refold the SOMAmer and dissociate any SOMAmer aggregates that may have formed during cold storage. We then centrifuged the solution at 6000 rpm for 10 s and added CRP to it. This LE-SOMAmer-CRP solution was immediately transferred from the tube to reservoir 4. We then applied a vacuum at reservoir 2 for 30 s, to fill the section of the channel between reservoir 4 and the intersection with LE, as well as the two analytes. We then rapidly rinsed the reservoir and replaced its contents with the TE buffer. Finally, we placed a positive electrode in reservoir 1 and ground in reservoir 4, and applied current (4 μA) to initiate ITP. As a result of the chemistry we used, the pH in ITP was between 7.2 and 7.7, depending on the zone.

Imaging System. For on-chip tracking of the ITP zone, we used an inverted epifluorescence microscope (Model Eclipse TE200, Nikon, Melville, NY) equipped with a 10× objective (Model PlanApo, Nikon, Melville, NY). We used a short-arc mercury lamp (Model 102DH, Ushio, Tokyo, Japan) and a filter cube optimized for AF488 detection (Model C-124352, Chroma, Bellows Falls, VT). We recorded all images using a 1300 × 1030 CCD camera (Coolsnap, Roper Scientific, Trenton, NJ) controlled with Winview32. Obtained images were processed with MATLAB software (R2011a, Mathworks, Natick, MA).

RESULTS AND DISCUSSION

Demonstration of Assay with CRP as a Target. For this initial demonstration, we chose CRP as a clinically relevant protein target. CRP is a pentameric protein commonly used as an inflammation biomarker. Its circulating plasma levels in healthy individuals are <80 nM, but can exceed 2 μM in severe bacterial infections.[39] CRP is also associated with myocardial disease.[40,41] In its nonglycosylated form, CRP has a molecular weight of 115 kDa[42] and an isoelectric point of 5−6.[43] The mobility of CRP varies significantly based on a number of factors, including pH and Ca^{2+} concentration.[38] Since the pH in the channel is between 7.2 and 7.7, above its isoelectric point, CRP is negatively charged under our assay conditions and migrates toward the cathode. However, reported mobility values of CRP indicate that it migrates relatively slowly (its mobility is reported as -1×10^{-9} m^2 V^{-1} s^{-1} at pH = 8.6, for example[44]). Therefore, we do not expect CRP to focus on ITP at either the LE/spacer or spacer/TE interfaces. Furthermore, low protein mobility often leads to low probe−target complex mobility and consequent higher value of α (see eq 7), allowing the complex to traverse the spacer zone and focus at the spacer/TE interface.

DOI: 10.1021/acs.analchem.5b00886
Anal. Chem. XXXX, XXX, XXX−XXX

In Figure 1b, we show experimental visualizations of SOMAmer fluorescence from the SOMAmer-CRP assay. In the negative control case, where no CRP is added, there is only one ITP peak, at the LE/spacer interface, corresponding to unbound SOMAmer. However, when CRP is added, a second peak forms at the spacer/TE interface, corresponding to SOMAmer−CRP complexes. We attribute the large axial width of the first ITP zone to the high concentration of Z-block (10 μM) used in the assay. Since Z-block is an oligodeoxynucleotide, it has mobility similar to that of the SOMAmer, and thus is focused at the LE/spacer interface.

Fraction of Focused SOMAmer in ITP. For the quantification experiments, we chose a probe concentration of 180 nM to minimize negative control signal (discussed below) and maximize fluorescent signal without saturating the detector. We measured the fluorescent signal at the detection point, located close to the cross junction. We chose this point because of the constraints imposed by the channel geometry. We found that this location maximized the accumulated fluorescent signal, while avoiding the perturbation caused by the cross junction and subsequent channel bending between the junction and reservoir 1 (see Figure 3). The number of focused unbound probe molecules at a given location along the channel is given by

$$N_P(x) = \left(\frac{\mu_P - \mu_{LE}}{\mu_{LE}}\right) c_P^{LE} A x \tag{8}$$

where x represents the axial location of the detection point along the channel. In this assay, the detection point, x_{det}, lies at ~90% of the injected plug length, L_0. For the low-target concentration case, the fraction of ITP-focused SOMAmers is estimated to be

$$\frac{N_P(x_{det})}{N_{P,o}} \approx 0.9\left(\frac{\mu_P - \mu_{LE}}{\mu_{LE}}\right) \approx 0.55 \tag{9}$$

Therefore, we estimate that we focused 55% of the available SOMAmers, based on our choice of detection point.

Fraction of Target-Bound SOMAmer. For each run, we measured the area-averaged fluorescent signal of the trailing ITP peak associated with the SOMAmer−CRP complex. We divided this value by the total fluorescent signal of the two ITP peaks. From this ratio, obtained for each sample, we subtracted the same signal ratio obtained for the negative control (which includes only probe and no protein target). As a result, we accounted for both run-to-run variation in injected SOMAmer and false positive fluorescent signal from the negative control. Finally, we normalized this number by the difference obtained for the case with excess target concentration (2 μM CRP). The raw data are included in the Supporting Information. We thus obtain the fraction of hybridized SOMAmer:

$$f_{complex} = \frac{\left(f_{p2}/f_{tot}\right) - \left(f_{c,p2}/f_{c,tot}\right)}{\left(f_{2uM,p2}/f_{2uM,tot}\right) - \left(f_{c,p2}/f_{c,tot}\right)} \tag{10}$$

Here, f_{p2}, $f_{c,p2}$, and $f_{2uM,p2}$ denote the area-averaged fluorescent signal observed in the trailing peak of the sample, control, and 2 μM runs, respectively. The parameters f_{tot}, $f_{c,tot}$, and $f_{2uM,tot}$ denote the combined area-averaged fluorescent signal observed in both ITP peaks, in the sample, control, and 2 μM runs, respectively.

We performed the normalization above in order to account for various factors that prevent the bound fraction of SOMAmers from reaching unity, even when CRP outnumbers SOMAmer by 10-fold. Such factors include protein aggregate formation, which we observed in the ITP zone during the runs with a CRP concentration of 2 μM. We hypothesize that this is due to the combination of high initial concentration of CRP and the preconcentration effects of ITP, which lead to CRP molecules aggregating and crashing out of solution. Other factors include wall adsorption and photobleaching.

Titration Curve and Limit of Detection. We built a titration curve using CRP as target and the CRP-specific SOMAmer as probe, shown in Figure 4. For all runs, we used a constant probe concentration of 180 nM and varied CRP concentration between 2 nM and 2 μM, performing three repetitions for each target concentration. In addition to the data points, we include a plot of the ITP hybridization model presented above (eqs 1 and 2). Because only the dissociation constant was known (K_d = 4 nM) rather than k_{on} or k_{off}, we use the kinetic on-rate as a free parameter to fit our model to the experimental data (we find $k_{on} = 3 \times 10^4$ M^{-1} s^{-1}). We find that the modified Damköhler number $\lambda \approx 3$ using the fitted value of k_{on}, placing the assay close to the optimal flat region shown in Figure 2. We achieve an LOD of 2 nM with a 2.5 decade dynamic range in a 10 min on-chip assay time. This result is comparable with that of Wang et al., who reported a limit of

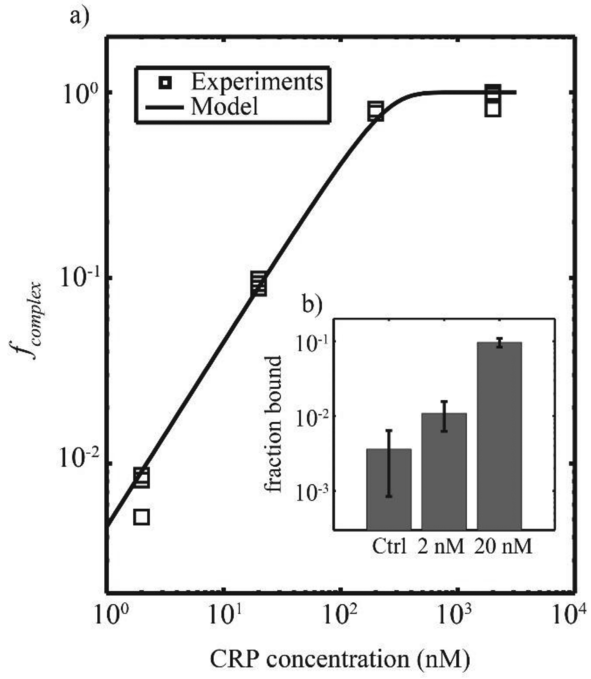

Figure 4. Experimental data of the ITP−spacer assay for the detection of CRP protein using CRP-specific SOMAmer. For all experiments, we fix the SOMAmer concentration at 180 nM. (a) Titration curve showing the control-corrected fraction of SOMAmer hybridized with increasing CRP concentration (from 2 nM to 2 μM). The assay has a 2.5 decade dynamic range (R^2 = 0.98). We also include a prediction of the model, using k_{on} as a fitting parameter ($k_{on} = 3 \times 10^4$ M^{-1} s^{-1}). (b) Limit of detection analysis that indicates a 2 nM limit of detection for this assay. The ratio of signal from the trailing peak to total signal is plotted for the negative control (c_T = 0) as well as the cases with two lowest CRP concentrations (c_T = 2 nM and 20 nM, respectively). Uncertainty bars represent 95% confidence on the mean.

DOI: 10.1021/acs.analchem.5b00886
Anal. Chem. XXXX, XXX, XXX−XXX

detection (LOD) of 1 nM for their t-ITP and aptamer-based detection assay. In addition, the reported LOD is well within the clinically relevant range of CRP, although we again stress that this LOD applies to our assay in a simple buffer, not in a complex sample.

CRP Detection in Serum. We explore the applicability of the CRP assay to complex samples. To this end, we performed preliminary experiments on diluted human serum. In addition to its high protein content, serum contains several anions that are present in millimolar concentrations, and thus form plateau-mode zones in ITP.[45,46] These anions, which include phosphate, sulfate, bicarbonate, and uric acid, have a wide range of mobilities. As a result, we observed additional spacer zones even after removing the original spacer ion (HEPES) from the TE buffer. We diluted the serum sample 20-fold in LE buffer to minimize protein aggregates and obtain higher sensitivity and repeatability. In diluted serum with spiked CRP target, our assay achieved an LOD of 25 nM, which is approximately an order of magnitude loss in sensitivity (see Figure S4 in the Supporting Information). We assume negligible levels of CRP naturally present in the serum samples. This limit of detection extrapolates to 500 nM in undiluted serum, a significant loss of clinical applicability for all but severe cases of inflammation. Clearly, additional work is required to extend our assay to clinical applications.

Extending this assay and other ITP reaction assays with proteins to a complex sample such as serum presents several challenges. As mentioned above, the presence of several ionic species in serum at high concentrations complicates an assay that is dependent on optimized buffer chemistry and species' mobilities. Another challenge is the abundance of other serum proteins, particularly albumin, which is present in very high concentration, and causes nonspecific binding to SOMAmer probes and other proteins; this is a well-known problem.[47,48] We hypothesize that nonspecific binding between SOMAmers and proteins increased our background fluorescence while preventing the binding of the SOMAmer to CRP. We note that the use of certain nonspecific competitors (such as Z-block) mitigates those effects (discussed in the Supporting Information). However, achieving specificity remains a difficult challenge. The high concentration of serum proteins also results in protein−protein interactions, leading to aggregate formation. We note that changing the surfactant from Tween-20 to Triton X-100 reduced aggregate formation in our experiments (see the Supporting Information). In addition, protein mobility is highly dependent on the local ionic and chemical environment. Unlike NAs, proteins have a wide range of isoelectric points and mobilities, which further complicates assay design in complex samples.

SUMMARY

We report here on our proof-of-concept effort toward extending ITP- and ionic spacer-based reaction and separation to the detection of protein targets. We introduce and discuss key parameters important in the design of an ITP-based reaction−separation assay where a low-mobility, nonfocusing target is recruited into ITP by a high-mobility probe. We then demonstrate our assay using the clinically relevant CRP protein. The assay is rapid, with 10 min off-chip heating plus 10 min on-chip ITP, and easy to implement with few manual steps. To our knowledge, this is the first ITP-based assay to show simultaneous on-chip reaction and separation of an aptamer and its protein target. Finally, we explore the extension of our assay to diluted serum spiked with CRP, where we encounter and discuss several challenges, including the formation of additional spacer zones and a loss of sensitivity.

The 2 nM LOD of the assay in clean buffer is acceptable for CRP detection, but needs to be improved for other clinically relevant protein targets. Our current assay had an extrapolated LOD of 500 nM in undiluted serum, which diminishes its clinical applicability. We hypothesize that using a custom-designed chip with a longer reaction zone or an aptamer with higher affinity would enhance sensitivity.

As discussed above, ITP assays accelerating NA reactions in complex samples have been successfully demonstrated and validated for several samples and applications. The narrow range of free-solution NA mobility[49] facilitates the exclusion of unwanted contaminants from the ITP zone. However, protein targets present additional challenges for ITP assays. Overcoming these challenges will require careful target selection and buffer chemistry design. We present this current work as an entry into extending ITP-based spacer assays to the detection of proteins and other low- or unknown-mobility targets, and as a guide for designing such assays.

ASSOCIATED CONTENT

Supporting Information

Additional information is noted in the text. The Supporting Information is available free of charge on the ACS Publications website at DOI: 10.1021/acs.analchem.5b00886.

AUTHOR INFORMATION

Corresponding Author

*Tel.: 650-723-5689. Fax: 650-723-7657. E-mail: juan.santiago@stanford.edu.

Author Contributions

The manuscript was written through contributions of all authors. All authors have given approval to the final version of the manuscript.

Notes

The authors declare no competing financial interest.

ACKNOWLEDGMENTS

This work was supported by a grant from Defense Advanced Research Projects Agency (DARPA), under Contract No. HR0011-12-C-0080. C.E. would like to thank the Gerald J. Lieberman fellowship for support.

REFERENCES

(1) Gold, L.; Walker, J. J.; Wilcox, S. K.; Williams, S. *Nat. Biotechnol.* **2012**, *29*, 543−549.
(2) Taguchi, A.; Hanash, S. M. *Clin. Chem.* **2013**, *59*, 119−126.
(3) Vidal, M.; Chan, D. W.; Gerstein, M.; Mann, M.; Omenn, G. S.; Tagle, D.; Sechi, S.; Workshop, P. *Clin. Proteomics* **2012**, *9*, 6.
(4) Anderson, N. L.; Anderson, N. G. *Mol. Cell. Proteomics* **2002**, *1*, 845−867.
(5) Surinova, S.; Schiess, R.; Huttenhain, R.; Cerciello, F.; Wollscheid, B.; Aebersold, R. *J. Proteome Res.* **2011**, *10*, 5−16.
(6) Gerszten, R. E.; Carr, S. A.; Sabatine, M. *Clin. Chem.* **2010**, *56*, 194−201.
(7) Liotta, L. A.; Petricoin, E. F. *Clin. Chem.* **2010**, *56*, 1641−1642.
(8) Jayasena, S. D. *Clin. Chem.* **1999**, *45*, 1628−1650.
(9) Ellington, A. D.; Szostak, J. W. *Nature* **1990**, *346*, 818−822.
(10) Tuerk, C.; Gold, L. *Science* **1990**, *249*, 505−510.
(11) Gold, L.; Ayers, D.; Bertino, J.; Bock, C.; Bock, A.; Brody, E. N.; Carter, J.; Dalby, A. B.; Eaton, B. E.; Fitzwater, T.; Flather, D.; Forbes, A.; Foreman, T.; Fowler, C.; Gawande, B.; Goss, M.; Gunn, M.; Gupta,

DOI: 10.1021/acs.analchem.5b00886
Anal. Chem. XXXX, XXX, XXX−XXX

S.; Halladay, D.; Heil, J.; Heilig, J.; Hicke, B.; Husar, G.; Janjic, N.; Jarvis, T.; Jennings, S.; Katilius, E.; Keeney, T. R.; Kim, N.; Koch, T. H.; Kraemer, S.; Kroiss, L.; Le, N.; Levine, D.; Lindsey, W.; Lollo, B.; Mayfield, W.; Mehan, M.; Mehler, R.; Nelson, S. K.; Nelson, M.; Nieuwlandt, D.; Nikrad, M.; Ochsner, U.; Ostroff, R. M.; Otis, M.; Parker, T.; Pietrasiewicz, S.; Resnicow, D. I.; Rohloff, J.; Sanders, G.; Sattin, S.; Schneider, D.; Singer, B.; Stanton, M.; Sterkel, A.; Stewart, A.; Stratford, S.; Vaught, J. D.; Vrkljan, M.; Walker, J. J.; Watrobka, M.; Waugh, S.; Weiss, A.; Wilcox, S. K.; Wolfson, A.; Wolk, S. K.; Zhang, C.; Zichi, D. *PLoS One* **2010**, *5*, e15004.

(12) Rohloff, J. C.; Gelinas, A. D.; Jarvis, T. C.; Ochsner, U. A.; Schneider, D. J.; Gold, L.; Janjic, N. *Mol. Ther.—Nucleic Acids* **2014**, *3*, e201.

(13) German, I.; Buchanan, D. D.; Kennedy, R. T. *Anal. Chem.* **1998**, *70*, 4540−4545.

(14) Pavski, V.; Le, X. C. *Anal. Chem.* **2001**, *73*, 6070−6076.

(15) Zhao, Q.; Li, X. F.; Le, X. C. *Anal. Chem.* **2008**, *80*, 3915−3920.

(16) Wang, L.; Ma, W.; Chen, W.; Liu, L.; Ma, W.; Zhu, Y.; Xu, L.; Kuang, H.; Xu, C. *Biosens. Bioelectron.* **2011**, *26*, 3059−3062.

(17) Wang, J.; Zhang, Y.; Okamoto, Y.; Kaji, N.; Tokeshi, M.; Baba, Y. *Analyst* **2011**, *136*, 1142−1147.

(18) Cheow, L. F.; Han, J. *Anal. Chem.* **2011**, *83*, 7086−7093.

(19) Garcia-Schwarz, G.; Rogacs, A.; Bahga, S. S.; Santiago, J. G. *J. Vis. Exp.* **2012**, e3890.

(20) Garcia-Schwarz, G.; Santiago, J. G. *Anal. Chem.* **2012**, *84*, 6366−6369.

(21) Garcia-Schwarz, G.; Santiago, J. G. *Angew. Chem., Int. Ed. Engl.* **2013**, *52*, 11534−11537.

(22) Bahga, S. S.; Han, C. M.; Santiago, J. G. *Analyst* **2013**, *138*, 87−90.

(23) Han, C. M.; Katilius, E.; Santiago, J. G. *Lab Chip* **2014**, *14*, 2958−2967.

(24) Khnouf, R.; Goet, G.; Baier, T.; Hardt, S. *Analyst* **2014**, *139*, 4564−4571.

(25) Kawabata, T.; Wada, H. G.; Watanabe, M.; Satomura, S. *Electrophoresis* **2008**, *29*, 1399−1406.

(26) Kagebayashi, C.; Yamaguchi, I.; Akinaga, A.; Kitano, H.; Yokoyama, K.; Satomura, M.; Kurosawa, T.; Watanabe, M.; Kawabata, T.; Chang, W.; Li, C.; Bousse, L.; Wada, H. G.; Satomura, S. *Anal. Biochem.* **2009**, *388*, 306−311.

(27) Bercovici, M.; Kaigala, G. V.; Mach, K. E.; Han, C. M.; Liao, J. C.; Santiago, J. G. *Anal. Chem.* **2011**, *83*, 4110−4117.

(28) Khurana, T. K.; Santiago, J. G. *Anal. Chem.* **2008**, *80*, 6300−6307.

(29) Martin, A. J.; Everaerts, F. M. *Anal. Chim. Acta* **1967**, *38*, 233−237.

(30) Khurana, T. K.; Santiago, J. G. *Anal. Chem.* **2008**, *80*, 279−286.

(31) Chambers, R. D.; Santiago, J. G. *Anal. Chem.* **2009**, *81*, 3022−3028.

(32) Eid, C.; Garcia-Schwarz, G.; Santiago, J. G. *Analyst* **2013**, *138*, 3117−3120.

(33) Bercovici, M.; Han, C. M.; Liao, J. C.; Santiago, J. G. *Proc. Natl. Acad. Sci. U.S.A.* **2012**, *109*, 11127−11132.

(34) Martin, A. J. P.; Everaert, F. M. *Proc. R. Soc. London, Ser. A* **1970**, *316*, 493−514.

(35) Bercovici, M.; Kaigala, G. V.; Backhouse, C. J.; Santiago, J. G. *Anal. Chem.* **2010**, *82*, 1858−1866.

(36) Hellman, L. M.; Fried, M. G. *Nat. Protoc.* **2007**, *2*, 1849−1861.

(37) Ruscher, K.; Reuter, M.; Kupper, D.; Trendelenburg, G.; Dirnagl, U.; Meisel, A. *J. Biotechnol.* **2000**, *78*, 163−170.

(38) Kraemer, S.; Vaught, J. D.; Bock, C.; Gold, L.; Katilius, E.; Keeney, T. R.; Kim, N.; Saccomano, N. A.; Wilcox, S. K.; Zichi, D.; Sanders, G. M. *PLoS One* **2011**, *6*, e26332.

(39) Clyne, B.; Olshaker, J. S. *J. Emerg. Med.* **1999**, *17*, 1019−1025.

(40) Ridker, P. M.; Haughie, P. *J. Invest. Med.* **1998**, *46*, 391−395.

(41) de Beer, F. C.; Hind, C. R.; Fox, K. M.; Allan, R. M.; Maseri, A.; Pepys, M. B. *Br. Heart J.* **1982**, *47*, 239−243.

(42) Pepys, M. B.; Hirschfield, G. M. *J. Clin. Invest.* **2003**, *111*, 1805−1812.

(43) Lee, M. H.; Lee, D. H.; Jung, S. W.; Lee, K. N.; Park, Y. S.; Seong, W. K. *Nanomedicine* **2010**, *6*, 78−83.

(44) Potempa, L. A.; Maldonado, B. A.; Laurent, P.; Zemel, E. S.; Gewurz, H. *Mol. Immunol.* **1983**, *20*, 1165−1175.

(45) Krebs, H. A. *Annu. Rev. Biochem.* **1950**, *19*, 409−430.

(46) Psychogios, N.; Hau, D. D.; Peng, J.; Guo, A. C.; Mandal, R.; Bouatra, S.; Sinelnikov, I.; Krishnamurthy, R.; Eisner, R.; Gautam, B.; Young, N.; Xia, J.; Knox, C.; Dong, E.; Huang, P.; Hollander, Z.; Pedersen, T. L.; Smith, S. R.; Bamforth, F.; Greiner, R.; McManus, B.; Newman, J. W.; Goodfriend, T.; Wishart, D. S. *PLoS One* **2011**, *6*, e16957.

(47) Travis, J.; Pannell, R. *Clin. Chim. Acta* **1973**, *49*, 49−52.

(48) Steel, L. F.; Trotter, M. G.; Nakajima, P. B.; Mattu, T. S.; Gonye, G.; Block, T. *Mol. Cell. Proteomics* **2003**, *2*, 262−270.

(49) Stellwagen, N. C.; Gelfi, C.; Righetti, P. G. *Biopolymers* **1997**, *42*, 687−703.

DOI: 10.1021/acs.analchem.5b00886
Anal. Chem. XXXX, XXX, XXX−XXX